Tropical Instability Waves at 0°N, 23°W in the Atlantic: A case study using PIRATA mooring data

Semyon A. Grodsky[1*], James A. Carton[1], Christine Provost[2], Jacques Servain[3,4], Joao A. Lorenzzetti[5], and Michael J. McPhaden[6]

Submitted to Journal of Geophysical Research - Oceans
March 1, 2005
Revised May 20, 2005

[1] Department of Atmospheric and Oceanic Science
University of Maryland
College Park, MD 20742, USA

[2] Laboratoire d'Océanographie Dynamique et de Climatologie (Paris),
Universite Paris VI, 4, Pl. Jussieu, 75252 Paris Cedex, France

[3] Institut de Recherche pour le Développement (IRD) - UR 065, France
Present affiliation:
[4] Fundação Cearense de Meteorologia e Recursos Hidricos (FUNCEME)
Av. Rui Barbosa, 1246
60115-121 - Fortaleza, CE, Brazil

[5] National Space Research Institute (INPE),
Remote Sensing Division
Av. Astronautas, 1758
12227-010 São José dos Campos, SP, Brazil

[6] NOAA/Pacific Marine Environmental Laboratory
7600 Sand Point Way NE
Seattle, WA 98115

* corresponding author senya@atmos.umd.edu

Abstract. Temperature, salinity, velocity, and wind from a mooring at 0^0 N, 23^0 W are used along with satellite sea surface temperature and sea level to examine the contribution of Tropical Instability Waves (TIWs) to the energy and heat balance of the equatorial Atlantic mixed layer. The TIWs appear as periodic 20-30 day fluctuations of currents, temperature, and salinity, which intensify beginning in June and peak in late boreal summer. The intensification occurs in phase with strengthening of the southeasterly trade winds and the seasonal appearance of the equatorial tongue of cold mixed layer temperatures. In 2002 these waves, which warm the mixed layer by 0.35^0 C during summer months, are maintained by both barotropic and baroclinic conversions that are of comparable size. Salinity fluctuations, previously neglected, increase the magnitude of baroclinic energy conversion.

1. Introduction.

A tongue of relatively cold water (<25^{o} C) enters the equatorial mixed layer in the eastern Atlantic in late boreal spring in response to intensified winds and a shallowing of the thermocline. This equatorial cold tongue, which plays a central role in the seasonal climate of the tropical Atlantic and eastern Pacific [*e.g. Okumura and Xie*, 2004], is separated from the warmer waters north of 5^{o} N by a strong narrow temperature front along the North Equatorial Countercurrent. In the mid-1970s *Duing et al.* [1975] and *Legeckis* [1977] observed that the meridional position of this temperature front undergoes intraseasonal fluctuations due to Tropical Instability Waves (TIWs) that have 20-30 day time-scales and 800-1000 km zonal space scales. The TIWs are now thought to play a key role in the heat budget of the tropical mixed layer [e.g. *Hansen and Paul*, 1984]. In this paper we present results from a new mooring deployment to examine the TIWs during 2002.

The energy source for TIWs has been linked to instabilities of the mean zonal currents [*Philander*, 1976]. In general, these waves extract energy through local interactions with the mean current and density fields via barotropic and baroclinic conversions [e.g. *Masina et al.*, 1999]. Discussions of the relative importance of barotropic and baroclinic energy conversions have a long history. Among those emphasizing barotropic processes, *Qiao and Weisberg* [1995] reported that phase lines associated with TIW velocity variation tilt against the meridional shear of zonal currents suggesting important barotropic conversions. More detailed observational analyses of *Weisberg and Weingartner* [1988] and *Qiao and Weisberg* [1998] and the model simulation study of *Jochum et al.* [2004] also suggest that barotropic instability of the

mean zonal currents is the primarily local source of energy for TIW. *Johnson and Proehl* [2004] have reported substantial correlation of TIW energy with the seasonal and interannual variation in strength of the near equatorial zonal currents.

While it is generally accepted that current shear (barotropic conversion) is an important source of the TIW energy, controversy exists over partitioning between the barotropic and baroclinic mechanisms. Several observational studies including *Hansen and Paul* [1984], *Luther and Johnson* [1990], and *Baturin and Niiler* [1997] have indicated a greater impact of the baroclinic instabilities on the TIW. In their model analyses *Masina et al*. [1999] and *Masina* [2002] have found a comparable contribution of the barotropic and baroclinic conversions, while *McCreary and Yu* [1992] have concluded that the baroclinic (frontal) instability is a leading source of the TIW energy. Finally to complicate matters, in his idealized model analysis *Proehl* [1996] has concluded that the TIWs extract energy from the background state through varying mixes of barotropic, baroclinic, and Kelvin-Helmholtz mechanisms.

One possible explanation for some of the variability among these studies is the fact that some studies, including *Weisberg and Weingartner* [1988], *Qiao and Weisberg* [1998], and *Jochum et al*. [2004] do not account for TIW-induced salinity fluctuations. These salinity fluctuations are significant [*McPhaden et al.,* 1984] and could affect the magnitude of the baroclinic conversion potentially significantly in the central Atlantic, where precipitation associated with the Intertropical Convergence Zone (ITCZ) largely controls the seasonal variations of salinity [*Dessier and Donguy,* 1994] and results in a persistent southward salinity gradient on the equator. Another possible explanation is that different mechanisms come into play under different mean conditions, perhaps explaining

the multiple frequency structure observed by *Lyman* [2003] and simulated by *Masina et al*. [1999]. Some observational support has been found in the equatorial Pacific by *Johnson and Proehl* [2004] who demonstrated that TIWs act to reduce both the shear of the large scale currents and their thermal structure, thus deriving energy from several source mechanisms. They also found that the partitioning between the mechanisms is zonally dependent with the contribution of the baroclinic conversions from sloping isopycnals increasing westward from 110^{o}W towards the date line.

As mentioned above, part of the interest in TIW dynamics lies in their potential contribution to the heat budget of the ocean mixed layer. Estimates of the magnitude of horizontal eddy heat advection of 100 W m^{-2} reported by *Hansen and Paul* [1984], *Bryden and Brady* [1989], *Weingartner and Weisberg* [1991], *Swenson and Hansen* [1999], and *Wang and McPhaden* [1999] are comparable to the seasonal variation of heat flux through the surface. On the other hand the observational analyses of *Weisberg and Qiao* [2000] and *Wang and Weisberg* [2001] show a strong interplay between the horizontal and vertical components of TIW heat advection that suggests an out-of-phase relationship between the two. Recently, *Vialard et al.* [2001] and *Jochum et al*. [2004] have questioned the contribution of the TIW to the mixed layer heat budget altogether. Based on modeling studies they suggest that warming by horizontal eddy heat advection is compensated for in part by cooling of the mixed layer by TIW-related entrainment. Previous observational estimates of the impact of TIW on the mixed layer heat balance that are based on the horizontal component only may thus be overestimated due to lack of contemporaneous vertical eddy fluxes.

In this paper we evaluate the energetics of the TIW and their contribution to the seasonal warming of the equatorial cold tongue mixed layer based on analysis of a new mooring data set (temperature, salinity, and velocity) collected at 0^0 N, 23^0 W in the tropical Atlantic during the year 2002. In addition to substantially increasing the available moored velocity observations in this basin the new observation set is enhanced by the availability of a number of additional contemporaneous (mostly satellite) observations that provide information on spatial fields needed to evaluate the eddy fluxes.

2. Data and Methods

The PIRATA (PIlot Research Array moored in the Tropical Atlantic) project is an international program (France, Brazil, and USA) http://www.brest.ird.fr/pirata/pirataus.html, which maintains a network of surface or near-surface measurements with the principal objective of describing and understanding the evolution of sea surface temperature (SST), upper ocean thermal structure and air-sea fluxes of momentum, heat and fresh water in the tropical Atlantic on the seasonal to interannual time scales [*Servain et al*., 1998]. The primary information used in this study comes from a combination of two moorings separated by ~ 3 km in the central equatorial Atlantic (0^oN, 23^oW). The first of these moorings is part of the original PIRATA array. At the first mooring temperature is recorded at 11 depths between 1 and 500 m with 20 m spacing in the upper 140 m, while salinity (via conductivity) is measured at four depths 1, 20, 40, and 120 m. Wind velocity is measured at 4 m above the sea surface.

At the second mooring an upward-looking Acoustic Doppler Current Profiler (ADCP) has provided currents during one year (13 December 2001 to 21 December 2002). The PIRATA current meter mooring was deployed in December 2001 from RV

ATALANTE and recovered in December 2002 from RV LE SUROIT. The near surface current meter was an upward looking Workhorse Sentinel Acoustic Doppler Current Profiler (RD Instruments ADCP 300 KHz). The data processing is detailed in *Kartavtseff and Provost* [2003]. The ADCP was located at 130 m depth (between 126.5 and 154.1 m) and provided profiles of the horizontal components of the velocity between 130 m and 12 m with a vertical resolution of 4 m and a time step of one hour. For the purpose of this study the original time series were averaged and decimated at daily interval. The velocity data are limited to depths below 12 m due to surface (reflection) effects, but continuous records during the whole observation period are available only between 16 m and 120 m depths (see **Figs. 1a, 1c**). The data availability of the temperature and salinity sensors at 0^{o}N, 23^{o}W during period of interest is shown in **Fig. 1e** and **Fig. 1f**, respectively. The primary observation set used in this analysis is this one-year long record of daily averaged temperature, salinity, and upward-looking ADCP velocity. Although vertical velocity was recorded, because of accuracy considerations only the horizontal component of velocity is used in this analysis.

In order to evaluate heat and momentum fluxes observations collected at the buoy site need to be complemented by horizontal gradients of temperature, salinity, and velocity within the mixed layer. Spatial fields of the SST have been provided by the Remote Sensing Systems at http://www.remss.com. We use 3-day average SST which is available on a 0.25^{o}x0.25^{o} grid from the Microwave Imager (TMI) aboard the US/Japanese Tropical Rainfall Measuring Mission satellite as a proxy for mixed layer temperature. The Microwave Imager (TMI) provides probably the most accurate SST for the tropical oceans because of the advantage of cloud transparency in the microwave

band. *Chelton et al*. [2001] have used TMI/SST to analyze surface signatures of TIW and discussed applicability of TMI/SST for TIW studies. *Gentemann et al*. [2004] have found a negligible bias and a standard deviation of 0.57 ^{o}C between the TMI/SST retrievals and in situ measurements in the tropical Pacific and Atlantic. Comparison of the TMI and PIRATA SSTs at 0^{o}N, 23^{o}W during 2002 shows a standard deviation of the difference of 0.3^{o}C throughout the year, increasing to 1^{o}C in boreal spring (**Fig. 2a**). During boreal spring the ITCZ is in its southern position, and a decrease in TMI/SST accuracy (some difference between TMI and observed SSTs may reach 2 ^{o}C) is explained by a reduction in data retrievals as the rain contaminated pixels are disregarded. Fortunately, as the ITCZ shifts south in boreal spring the SST gradient weakens thus decreasing an impact of increasing SST errors on the heat flux and eddy energy flux estimates.

We rely on the climatological monthly estimates of Sea Surface Salinity of *Dessier and Donguy* [1994] available on a 1^{o}x1^{o} grid. *Foltz et al*. [2004] have shown that the gradient of this climatological SSS provides a reliable estimate of salt advection in the western tropical Atlantic. In the eastern Atlantic, where precipitation associated with the Intertropical Convergence Zone (ITCZ) and African river discharges largely control the seasonal variations of SSS [*Dessier and Donguy*, 1994], the seasonal variations of salinity gradient is also well captured by the SSS climatology. These estimates are consistent with PIRATA observations in boreal summer (**Fig. 2b**) but underestimate the near surface freshening in boreal spring. This underestimation should have a little impact on the eddy fluxes estimate because these fluxes are weak during March- May (see **Fig. 6b** below).

Computation of near surface velocity fields also poses a challenge. We use the altimeter-based AVISO geostrophic currents that provide spatial resolution of 0.3^ox0.3^o over the tropical oceans at weekly intervals. In the AVISO data (available at http://las.aviso.oceanobs.com/las/servlets/dataset), geostrophic zonal velocities at the equator are computed from sea level, η, assuming a balance between the meridional curvature of pressure and the β-effect [*Picaut et al*., 1989; *Menkes et al*. 1995], $u = -g/\beta \partial^2 \eta / \partial y^2$, [AVISO team personnel communication], while outside a 5° band around the equator the flow is assumed fully geostrophic. In a 5° a band around the equator, a connection is computed to ensure continuity with classical geostrophy following *Carton and Hackert* [1989]. The details of the AVISO currents retrieval and data quality assessment have not been published yet. To compare the AVISO currents with the PIRATA measurements we assume that the near surface currents can be decomposed into a geostrophic and wind driven components. We estimate the wind driven component of currents on the equator using the PIRATA wind stress, $\boldsymbol{\tau}$, and the simple frictional model of *Cane* [1980], in which the friction is parameterized by Raleigh linear damping term, $r\mathbf{U}_w$, that balances the wind stress on the equator.. In **Fig. 2c** the PIRATA zonal geostrophic currents are calculated by subtracting the wind driven zonal component, $u_w = \tau_x / \rho r H$, averaged over the upper H =40 m with a frictional timescale, r, and a drag coefficient of 2 days and $1.2\text{x}10^{-3}$, respectively. Although the discrepancy between the two independent estimates of geostrophic currents is noticeable in January and June, they have similar seasonal variations and capture surfacing of the eastward currents in March-April, westward currents strengthening in June (in phase with the onset of TIW season), and relatively weak zonal currents on the equator beginning August [see

also *Provost et al*, 2004 for further comparisons of the PIRATA currents and altimeter data].

Horizontal gradients of temperature, salinity, and velocity are used to estimate the TIW energy balance and TIW induced heat flux. To evaluate the TIW energy balance we separate all variables into low and high frequency components. Here and after a high frequency component (denoted by a prime) is defined as the deviation from the running mean and is obtained by filtering out the low frequency component with a running mean rectangular filter whose width, *W*, will be specified later. The equation for eddy (TIW) energy balance is given by [see *e.g. Brooks and Niiler*, 1977]:

$$dE/dt = -\rho\langle \mathbf{u}' \cdot (\mathbf{u}' \cdot \nabla \mathbf{U}) \rangle - g\langle \rho' \mathbf{u}' \cdot \nabla_H \rho \rangle / |\rho_z| - \langle \nabla \cdot (\mathbf{u}' p') \rangle, \qquad (1)$$

where $E = \rho\langle \mathbf{u}'\mathbf{u}' \rangle / 2 + g\langle \rho'^2 \rangle / (2|\rho_z|)$. Terms of order three and higher are omitted and standard notations are used in (1). The subscript *H* indicates horizontal derivative, angular brackets and the terms without upper prime denote running mean.

We are unable to estimate all terms in (1), so we need to rely on a number of simplifying assumptions. The first term on the right-hand side of (1) describes the eddy energy production by Reynolds stresses acting against the current shear. This term includes the part proportional to the horizontal current shear (barotropic conversion) and the part proportional to the vertical shear (Kelvin-Helmholtz conversion). We neglect the Kelvin-Helmholtz conversion because vertical velocity isn't available and because this conversion contributes mainly to daily and shorter fluctuations. We also disregard the barotropic conversion terms involving zonal current derivatives based on the scaling analysis of *Luther and Johnson* [1990]. The second term on the right-hand side of (1) describes the eddy energy production by the eddy buoyancy fluxes acting on the density

gradient (baroclinic conversion). The third term on the right-hand side of (1) is the pressure work done by eddies. It redistributes the eddy energy spatially and drops out when averaged over the volume [*Mazina et al.*, 1999]. Under these simplifications (1) is written as (2) where only the barotropic conversion due to meridional shear (line 1) and the baroclinic conversion (line 2) are retained

$$\begin{aligned} dE/dt = &-\rho\langle u'v'\rangle U_y - \rho\langle v'v'\rangle V_y + \\ &- g\langle u'\rho'\rangle\rho_x / |\rho_z| - g\langle v'\rho'\rangle\rho_y / |\rho_z| \end{aligned} \qquad (2)$$

We average the terms in (2) vertically through the upper 40-m water, a depth that roughly coincides with the mixed layer depth at the mooring location and spans 3 upper measurement levels. The vertical density derivative, ρ_z, is then estimated as the central difference between z=40m and z=1m levels. Calculations are done for a number of the filter widths W=20 to 40dy. These multiple calculations give an assessment of the results as a function of the filter width, W.

Meridional shear of the zonal current in (2) is calculated as the sum of geostrophic and wind driven components, while it is assumed that the meridional divergence is dominated by wind driven component. Due to β-effect, even homogeneous wind over the equator produces the meridional divergence, $\partial V_w / \partial y = -\beta\tau_x / (\rho r^2 H)$, and the meridional shear, $\partial U_w / \partial y = \beta\tau_y / (\rho r^2 H)$, assuming the wind related stress, $\boldsymbol{\tau}$, vanishes at the bottom of the upper H=40m layer.

The terms of the TIW energy balance equation (2) are estimated as mean values in the upper ocean 40 m. Velocity information is available only below 16m. Because of that we have to make an assumption to relate velocity fluctuation above and below the upper measurement level. Fortunately, an Empirical Orthogonal Function analysis of the

velocity data (**Fig 3a)** shows that neither component varies strongly with depth over the depths we have observations. Therefore we assume the velocity fluctuations are depth independent in the upper 40m.

A final issue that needs to be addressed is the data dropout in June. During the first half of 2002 all three temperature and salinity sensors in the upper 40 m column were operational, but the 20 m sensors broke in June (**Figs. 1e, 1f**). To account for missing data a correlation of temperature and salinity variations between z=20m and z=1m was calculated using data for other years. These correlations exceed 0.8, and data scatter around the diagonals corresponding to equal variations at z=1m and z=20m depths (**Figs. 3b, 3c**). Based on this comparison the gap at 20m depth was filled using the 1m observations.

3. Results

We begin by examining the background velocity observed at 0^o N, 23^o W (**Figs. 1a, c**). The velocity record for the year 2002 shows a modest westward flowing South Equatorial Current (SEC) with a mean current of ~20 cm s^{-1} at 16m depth (**Fig. 1b**). The SEC is present within the 30-50 m depth mixed layer except in boreal spring. Below the mixed layer in the thermocline there is an intense eastward flowing Equatorial Undercurrent (EUC) whose mean velocity is 80 cm s^{-1} (**Fig. 1b**) that may exceed 110 cm s^{-1} at ~80 m depth (**Fig. 1a**). In boreal spring in response to the easterly wind weakening, the EUC shallows causing the appearance of eastward currents along with warm temperatures in the mixed layer (**Figs. 1a, 1e**). Shallowing of the EUC increases the

salinity of the lower mixed layer (**Fig. 1f**). But in the upper 20 m increased precipitation leads to freshening.

In contrast to the seasonal zonal currents, the meridional currents at 0^o N, 23^o W are dominated by intraseasonal variations (**Fig. 1c**), with a mean southward flow from z=16m to 80m (**Fig. 1d**). This southward flow is highest, 8cm s^{-1}, just below the mixed layer at 50 m depth. Both zonal and meridional mean currents and their standard deviations are similar to that reported for the year 1981 by *Weisberg* [1985] at 0^o N, 28^o W (**Figs. 1b, d**).

In boreal summer the intraseasonal oscillations of meridional velocity, which are present year-round, strengthen. Interestingly, the meridional velocity fluctuations vary coherently throughout the upper 120 m of the water column (vertical coherence in the 20 day - 40 day band exceeds 0.6), while the zonal velocity fluctuations are coherent only within the mixed layer. Fluctuations in zonal velocity are largest in June-July, while fluctuations in meridional velocity are largest in August-September (**Figs. 1a, c**). These intraseasonal velocity fluctuations are accompanied by pronounced fluctuations of salinity at the buoy location (**Fig. 1f**) while the intraseasonal fluctuations of temperature are less evident (**Fig. 1e**). These fluctuations of temperature occur approximately two months later in the year than fluctuations previously observed at 0^o N, 28^o W during the year of 1983 by *Weisberg and Weingartner* [1988] indicating that the seasonal phase of the TIW can vary significantly in the Atlantic.

During June - September five TIW events are evident in **Fig. 4**. These events result from arriving of TIW crests, which propagate westward at phase speed 40 ± 4 cm s^{-1} as estimated from the longitude/time diagram of the TMI/SST at 2^o N (plus/minus

bounds the scatter in speed of individual TIWs). At 16m depth the summer time velocity fluctuations typically consist of a southward anomaly of 0.5 m s^{-1} and a westward surge of comparable magnitude (see **Fig. 4a**) suggesting the NE-SW orientation of the velocity fluctuation ellipses. For the five TIW events in June-September the horizontal velocity components fluctuate almost in phase. Cross-correlation analysis of the horizontal velocity fluctuations during June – September (not shown) indicates that the meridional component, v', slightly leads the zonal component, u', by ~ 3 days.

Salinity throughout the mixed layer varies in phase with changes in meridional velocity (**Figs. 1c, 1f, 4b, 4d**), apparently determined by meridional excursions of the seasonal salinity gradient (fresher water to the north) due to TIW. Temperature fluctuations are also evident in the summer months (**Figs. 4a**), however they are not as well correlated with meridional velocity fluctuations, and thus contribute less to the meridional eddy buoyancy flux (hence, baroclinic conversion). During the four-month period June-September a succession of five TIW events takes place. Increases in temperature at the mooring site occur for three of the five TIW events with an average increase of ~2^{o}C. During the other two (indicated by an '*o*' in **Fig. 4a**) there was essentially no local temperature increase.

We next consider temporal changes of the TIW beginning with the eddy kinetic energy (**Fig.5a**). Zonal velocity covariance peaks in June-July leading by a month the peak in meridional covariance that occurs in August. The Reynolds stress increases in magnitude in June (**Fig. 5b**) following the strengthening of the cyclonic meridional shear of the zonal currents in May and remains high until September (**Fig. 5c**). The Reynolds

stress is mostly confined to the mixed layer and the upper thermocline confirming that the energy transfer is occurring at these depths.

To evaluate the importance of Kelvin-Helmholtz instability to energy budget of the TIW we estimate the bulk Richardson number, Ri_b, based on the PIRATA temperature, salinity, and velocity measurements in the mixed layer and the depth of the core of the EUC. Throughout the year Ri_b remains larger than the critical value of 0.25 suggesting a minor (if any) impact of the Kelvin-Helmholtz instability on the TIW energy budget.

Barotropic energy conversion occurs in response to cyclonic shear of the mean zonal currents (**Fig. 6a**). This term is positive in boreal summer and increases again in boreal winter. It dominates eddy energy dissipation produced by the meridional velocity divergence.

Next we consider an impact of salinity observations on the baroclinic energy conversion estimate. Accounting for salinity affects the magnitude of baroclinic conversion in two ways, by affecting the background density gradient, and by affecting the buoyancy flux. Salinity fluctuation occurs in-phase with velocity fluctuation (**Fig. 4**), hence contributes to the buoyancy flux. To estimate the effect of salinity on the magnitude of baroclinic conversions, we first begin with the estimate of density fluctuation, ρ', and background density gradient, $\nabla_H \rho$, based on the temperature only. This approach may underestimate the buoyancy flux, $-g<\rho'\mathbf{u}'>$, given differences in TIW-induced fluctuation of temperature and salinity (**Figs. 4a, 4b**), as well as underestimate the background isopycnal slope. If salinity fluctuations are neglected in the evaluation of the baroclinic conversion terms, the zonal, $-g<u'\rho'>\rho_x/|\rho_z|$, and the

meridional, $-g<v'\rho'>\rho_y/|\rho_z|$, components almost cancel each other (**Fig. 6b**) as has been found previously by *Weisberg and Weingartner* [1988]. When salinity is included, however, the meridional term increases substantially thus unbalancing the terms and increasing the magnitude of the total baroclinic conversion. As a result, the baroclinic conversion becomes comparable in size to the barotropic conversion (**Fig. 6c**). Little effect of salinity on the zonal component of the baroclinic conversion is explained in part by the horizontal salinity gradient which is primarily meridional [*Dessier and Donguy*, 1994] in the eastern equatorial Atlantic and, hence has a little impact on the background zonal density gradient.

We next consider the contribution of the TIW to the seasonal mixed layer heat budget. Increases in temperature at the buoy site occur for three of the five TIW events (marked by '+') with an average increase of 2^o C (**Fig. 4**). During the other two (marked by 'o') there was essentially no local temperature increase. To understand differences in SST response to individual TIW events we turn our attention to horizontal heat advection, which is the scalar product of the gradient of mixed layer temperature and horizontal velocity. Heat advection is an important term of the heat balance of the equatorial mixed layer. *Wang and Weisberg* [2001] have found that in the central Pacific roughly half of the SST variation at intraseasonal time scale is accounted for by the heat advection. At the buoy location we compare 3-day mean rate of change of the mixed layer heat content and the heat advection (**Fig. 7**) and find that the advection term accounts for 52% of the heat content variance in close agreement with the previous estimate.

To assess differences in heat advection for individual TIWs we compare the geographic orientation of the mixed layer velocity and the thermal front during two

events #1 and #2 (see **Fig. 4a** for numbering). During these two events the magnitude of the velocity fluctuations are similar (**Figs. 4c, 4d**) but the temperature fluctuations differ substantially. Overlaying the velocity on the SST fields, we find in **Fig. 8a** that the velocity fluctuation is oriented parallel to isotherms during event #1. Moreover, the buoy is located within the equatorial cold tongue where the SST gradient is weaker in comparison to the northern edge of the cold tongue. Under these conditions, as in event #1, warming is weak (see **Figs. 4a, 8a**). In contrast, during event #2 the mixed layer temperature gradient is almost northward while the currents are southwestward (**Fig. 8b**). During event #2 the buoy is at the northern edge of the equatorial cold tongue where the magnitude of SST gradient is larger than in the interior of the cold tongue. In this case temperature advection is large and warming at the mooring site significant.

In contrast to the southward surges of events #1 and #2, northward surges cause SST to drop to the temperature of the equatorial cold tongue and so the gradient of temperature becomes weak. This asymmetry allows velocity fluctuation to induce substantial eddy horizontal heat advection, $-C_p \rho H < \mathbf{u}' \cdot \nabla T' >$. In present study we find one of the order of 100 W m^{-2} in the upper H=50 m in line with previous studies [see e.g. *Weisberg and Weingartner,* 1988]. This strong horizontal eddy heat advection may be balanced by vertical eddy flux convergence or by mixed layer warming tendency. We evaluate the seasonal warming due to individual TIW comparing the SST to the value it would have in the absence of TIW as estimated by the linear interpolation of SST between the beginning and end of each TIW warm event (shown in **Fig. 4a**). We assume that the TIWs affect SST only during the warm events (shaded in gray). The seasonal average of SST is higher during boreal summer by 0.35^0 C when we include the gray

shaded regions in the average versus than if we did not. Thus, the increase in seasonal SST due to the TIWs is 0.35^{o} C translating into a convergence of eddy heat flux of 10 W m^{-2} in the upper 50 m. This estimate of heat storage rate is very much less than direct estimates of the horizontal eddy heat advection [see e.g. *Weisberg and Weingartner*, 1988]. Together these case results are in accord with the conclusion of *Vialard et al.* [2001] and *Jochum et al.* [2004] who suggest that cooling due to vertical eddy heat advection compensates for warming due to horizontal eddy heat advection, and the net impact of the TIW on the heat budget of the equatorial mixed layer is weak.

4. Summary

The TIW appear as periodic 20-30 day fluctuations in currents which develop beginning June in phase with the strengthening of the southeasterly trades and the seasonal appearance of cool < 24^{o} C mixed layer temperatures along the equator. We use temperature, salinity, and velocity time series from two moorings both located at 0^{o}N, 23^{o}W for one year (December 2001 – December 2002) along with complimentary satellite and climatological data to evaluate some of the features of Tropical Instability Waves, including the barotropic and baroclinic conversions in the TIW energy budget, and assess the role of TIW in the mixed layer heat balance in this region of the equatorial Atlantic.

We begin by examining the phase relationship among variables. Zonal current fluctuations are stronger in June-July while meridional fluctuations persist throughout the year, reaching their maximum in August-September. Fluctuations of both current components are of similar amplitude (0.5 m s^{-1}). The meridional velocity fluctuations

vary coherently throughout the upper 120 m (the whole water column of ADCP ovservations), while the zonal velocity fluctuations are coherent only within the mixed layer. These vertical structures are very similar to those for instability waves of similar periods in the central Pacific a 0^{o}N, 140^{o}W [*McPhaden,* 1996]. Some, but not all of the fluctuations result in fluctuations of the mixed layer temperature. In contrast, fluctuations of mixed layer salinity are well correlated with fluctuations of current and occur in-phase with the meridional velocity fluctuations.

We next consider the TIW energy budget. We find that accounting for observed salinity fluctuations (neglected in some previous studies) increases our estimate of baroclinic energy conversion by a factor of three. As a result, we find barotropic and baroclinic conversions are similar in magnitude suggesting that the both maintain the TIWs in the central equatorial Atlantic during boreal summer.

Finally we consider the contribution of TIW to the seasonal heat budget. The summer contribution of the TIW to warming of the mixed layer is found to be quite small (10 W m^{-2}). This modest storage rate is very much less than estimates of previous studies of the summer contribution of TIW to convergence of horizontal eddy heat flux. This inconsistency indicates that the vertical eddy heat advection must balance horizontal eddy heat advection, thus reducing the impact of TIW on the heat budget of the equatorial cold tongue.

Acknowledgments. Data management is conducted by the TAO Project Office at NOAA/PMEL in collaboration with many research Institutes listed on the PIRATA web site at http://www.pmel.noaa.gov/pirata. This work was supported by the French Ministry

of Research (ACI Climat), by NOAA's Office of Oceanic and Atmospheric Research and Office of Global Programs, by the National Science Foundation, by the IRD (Institut de Recherche pour le Développement), by CNES (Centre National de Recherche Spatiale), by Météo-France, by Institut National des Sciences de l'Univers (INSU Convention N 01CV071), and by National Space Research Institute (INPE), Brazil. The ADCP mooring opportunity was the result of French-Brazilian cooperation within the PIRATA project. The ADCP data were processed and validated at Laboratoire d'Océanographie Dynamique et de Climatologie (LODYC, Paris). The ADCP data are available at http://www.pmel.noaa.gov/tao/data_deliv/deliv-pir.html. We deeply acknowledge the help of the Lanoisellé family and crew members from R.V. Atalante and R.V. Le Suroit for mooring construction, deployment and recovery. We are grateful to M. Jochum formerly of MIT, J. Lyman of NOAA/PMEL, and anonymous reviewers for comments on the original manuscript. TMI/SST data are produced by Remote Sensing Systems. The altimeter products were produced by SSALTO/DUACS and distributed by AVISO, with support from CNES, France.

References.

Baturin, N. G., and P. P. Niiler, Effects of instability waves in the mixed layer of the equatorial Pacific, *J. Geophys. Res.*, *102*, 27,771-27,793, 1997.

Bryden, H., and E. C. Brady, Eddy momentum and heat fluxes and their effect on the circulation of the equatorial Pacific Ocean, *J. Mar. Res., 47*, 55-79, 1989.

Brooks, I. H., and P. P. Niiler, Energeticts of the Florida Current, *J. Mar. Res., 35*, 163-191, 1977.

Cane, M., On the dynamics of the equatorial currents, with application to the Indian Ocean, *Deep Sea Res., 27*, 524-544, 1980.

Carton, J.A., and E.C. Hackert, Application of multi-variate statistical objective analysis to the circulation in the tropical Atlantic ocean, *Dyn. Atm. Ocean., 13,* 491-515, 1989.

Chelton, D. B., S. K. Esbensen, M. G. Schlax, N. Thum, M. H. Freilich, F. J. Wentz, C. L. Gentemann, M. J. McPhaden, and P. S. Schopf. Observations of coupling between surface wind stress and sea surface temperature in the eastern Tropical Pacific, *J. Climate*, *14,* 1479 -1498, 2001.

Dessier, A., and J. R. Donguy, The sea surface salinity in the tropical Atlantic between 10S and 30N - seasonal and interannual variations (1977 - 1989), *Deep Sea Res.*, *41*, 81-100, 1994.

Duing, W., P. Hisard, E. Katz, J. Meincke, L. Miller, K. V. Moroshkin, G. Philander, A. A. Ribnikov, K. Voit, and R. Weisberg, Meanders and long waves in equatorial Atlantic, *Nature*, *257*, 280-284, 1975.

Foltz, G.R., S.A. Grodsky, J.A. Carton, and M.J. McPhaden, Seasonal salt budget of the northwestern tropical Atlantic Ocean along 38^{o} W, *J.Geoph. Res., 109*, C03052, doi:10.1029/2003JC0021112004, 2004.

Gentemann, C.L., F.J. Wentz, C.A. Mears, and D.K. Smith, In situ validation of Tropical Rainfall Measuring Mission microwave sea surface temperatures, *J. Geophys. Res*., 109, C04021, 2004.

Hansen, D., and C. Paul, Genesis and the effect of long waves in the equatorial Pacific, *J. Geophys. Res*., *89*, 10,431-10,440, 1984.

Jochum, M., P. Malanotte-Rizzoli, and A. Busalacchi, Tropical instability waves in the Atlantic Ocean, *Ocean Modelling*, *7*, 145-163, 2004.

Johnson, E.S., and J.A. Proehl, Tropical instability wave variability in the Pacific and its relation to large-scale currents, *J. Phys. Oceanogr.*, *34*, 2121-2147, 2004.

Kartavtseff, A., and C. Provost, Mouillages courantométriques PIRATA Décembre 2001-Décembre 2002, *Rapport interne LODYC* #2003-01, 128 pp., 2003.

Legeckis, R., Long waves in eastern equatorial Pacific ocean - view from a geostationary satellite, *Science*, *197*, 1179-1181, 1977.

Luther, D. S., and E. S. Johnson, Eddy energetics in the upper equatorial Pacific during the Hawaii-to-Tahiti shuttle experiment, *J. Phys. Oceanogr*, *20*, 913-944, 1990.

Lyman, J. M., Separating 20 and 30 day Tropical Instability Waves in the central Pacific, *EOS Trans. AGU*, *84*(52), Ocean Sci. Meet. Suppl., Abstract OS51K-01, 2003.

Masina, S., S. G. H. Philander, and A. Bush, An analysis of tropical instability waves in a numerical model of the Pacific Ocean, 2. Generation and energetics of the waves, *J. Geophys. Res*., *104*, 29613-29635, 1999.

Masina, S., Instabilities of continuously stratified zonal equatorial jets in a periodic channel model, *Annal. Geophys.*, *20*, 729-740, 2002.

McCreary, J. P., and Z. Yu. Equatorial dynamics in a 2½-layer model, *Prog. Oceanogr*., *29*, 61-132, 1992.

McPhaden, M. J., M. Fieux, and J. Gonella, Meanders observed in surface currents and hydrography during an equatorial Atlantic transect, *Geoph. Res. Lett*., *11*, 757-760, 1984.

McPhaden, M. J., Monthly period oscillations in the Pacific North Equatorial Countercurrent. *J. Geophys. Res*., *101*, 6337-6359, 1996.

Menkes, C., J.-P. Boulanger, and A.J. Busalacchi, Evaluation of TOPEX and basin-wide Tropical Ocean and Global Atmosphere-Tropical Atmosphere Ocean sea surface topographies and derived geostrophic currents, *J. Geophys. Res*., *100*, 25,087-25,099, 1995.

Okumura, Y., and S.P. Xie, Interaction of the Atlantic equatorial cold tongue and the African monsoon, *J. Clim.*, *17*, 3589-3602, 2004.

Philander, S. G. H., Instabilities of zonal equatorial currents, *J. Geophys. Res.*, *81*, 3725-3735, 1976.

Picaut, J., S. P. Hayes, and M. J. McPhaden, Use of geostrophic approximation to estimate time-varying zonal currents at the equator, *J. Geophys. Res., 94*, 3228-3236, 1989.

Proehl, J. A., Linear stability of equatorial zonal flows, *J. Phys. Oceanogr., 26*, 601-621, 1996.

Provost, C., S. Arnault, N. Chouaib, A. Kartavtseff, L. Bunge and E. Sultan, Equatorial pressure gradient in the Atlantic in 2002: TOPEX Poseidon and Jason versus the first PIRATA current measurements, *Marine Geodesy, 27*, 13774-13769, 2004.

Qiao, L., and R. H. Weisberg, Tropical Instability Waves kinematics: Observations from the Tropical Instability Wave Experiment, *J. Geophys. Res., 100*, 8677-8693, 1995.

Qiao, L., and R. H. Weisberg, Tropical instability wave energetics: Observations from the tropical instability wave experiment, *J. Phys. Oceanogr, 28*, 345-360, 1998.

Servain, J., A. J. Busalacchi, M. J. McPhaden, A. D. Moura, G. Reverdin, M. Vianna, and S. E. Zebiak, A Pilot Research Moored Array in the Tropical Atlantic (PIRATA), *Bull. Amer. Meteorol. Soc., 79*, 2019-2031, 1998.

Swenson, M. S., and D. V. Hansen, Tropical Pacific ocean mixed layer heat budget: The Pacific cold tongue, *J. Phys. Oceanogr., 29*, 69-81, 1999.

Vialard, J., C. Menkes, J.-P. Boulanger, P. Delecluse, E. Guilyardi, M. J. McPhaden, and G. Madec, A model study of oceanic mechanisms affecting equatorial Pacific sea surface temperature during the 1997-98 El Niño, *J. Phys. Oceanogr., 31*, 1649-1675, 2001.

Wang, W., and M.J. McPhaden, The surface layer heat balance in the equatorial Pacific Ocean, Part I: Mean seasonal cycle, J. Phys. Oceanogr., 29, 1812-1831, 1999.

Wang, C. Z., and R. H. Weisberg, Ocean circulation influences on sea surface temperature in the equatorial central Pacific, *J. Geophys. Res., 106*, 19515-19526, 2001.

Weingartner, T. J., and R. H. Weisberg, A description of the annual cycle in sea surface temperature and upper ocean heat in the equatorial Atlantic, *J. Phys. Oceanogr., 21*, 83-96, 1991.

Weisberg, R.H., Equatorial Atlantic velocity and temperature observations - February-November 1981, *J. Phys. Oceanogr., 15*, 533-543, 1985.

Weisberg, R. H., and T. J. Weingartner, Instability waves in the equatorial Atlantic-ocean, *J. Phys. Oceanogr., 18*, 1641-1657, 1988.

Weisberg, R. H., and L. Qiao, Equatorial upwelling in the central Pacific estimated from moored velocity profilers, *J. Phys. Oceanogr., 30*, 105-124, 2000.

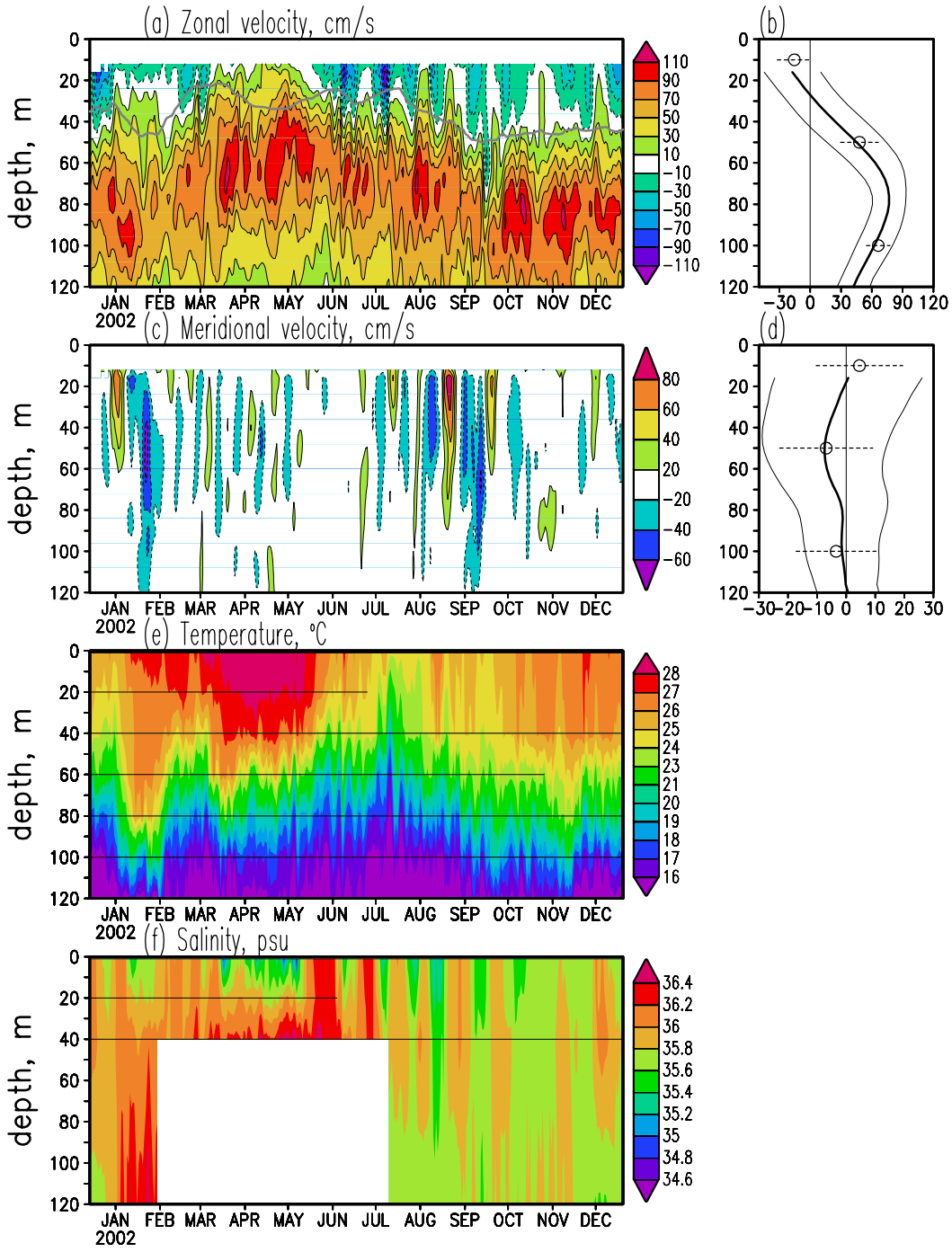

Figure 1. Data from 0° N, 23° W moorings. (a) Zonal and (c) meridonal velocity. Gray line in (a) is the mixed layer depth (calculated as the depth where temperature is 1^0 C below the night-time SST). Tick marks along the time axes denote the first day of the month. Mean (b) zonal (d) meridional currents (bold). Thin lines in (b,d) bound the standard deviation of daily currents. Also shown are mean currents (open circles) and standard deviation of currents (horizontal dashed) for 1981 [*Weisberg*, 1985]. (e) Temperature and (f) salinity from the PIRATA ATLAS mooring. Horizontal lines in (e, f) indicate the data availability at particular level.

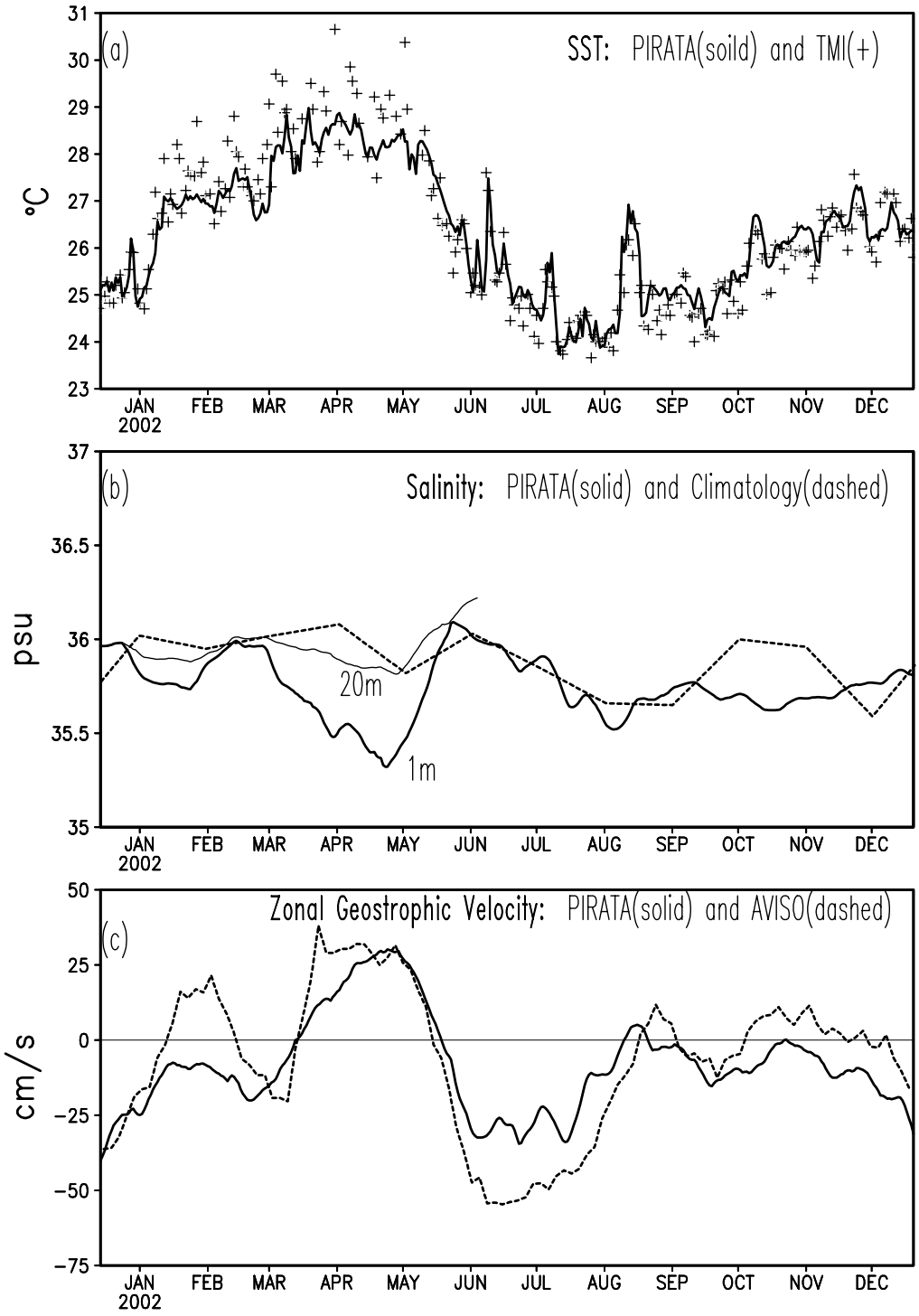

Figure 2. Comparison of (a) PIRATA and TMI 3-day averaged SST, (b) PIRATA monthly running mean salinity at 1m and 20m depths and climatological monthly surface salinity, (c) monthly running mean zonal geostrophic currents from PIRATA and AVISO altimetry.

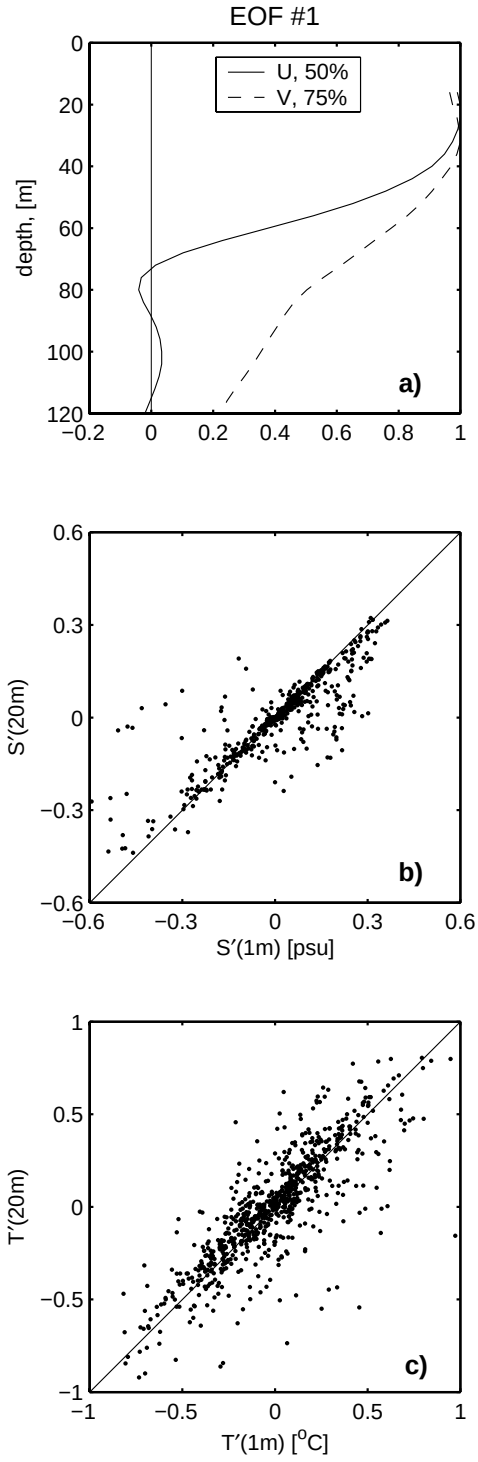

Figure 3. (a) Leading vertical EOF of the intramonth zonal and meridional velocity fluctuations (numbers in the legend are percent of explained variance). (b,d) Comparison of the intramonth fluctuations of temperature and salinity at the near surface (z=1m) and mixed layer (z=20m) horizons.

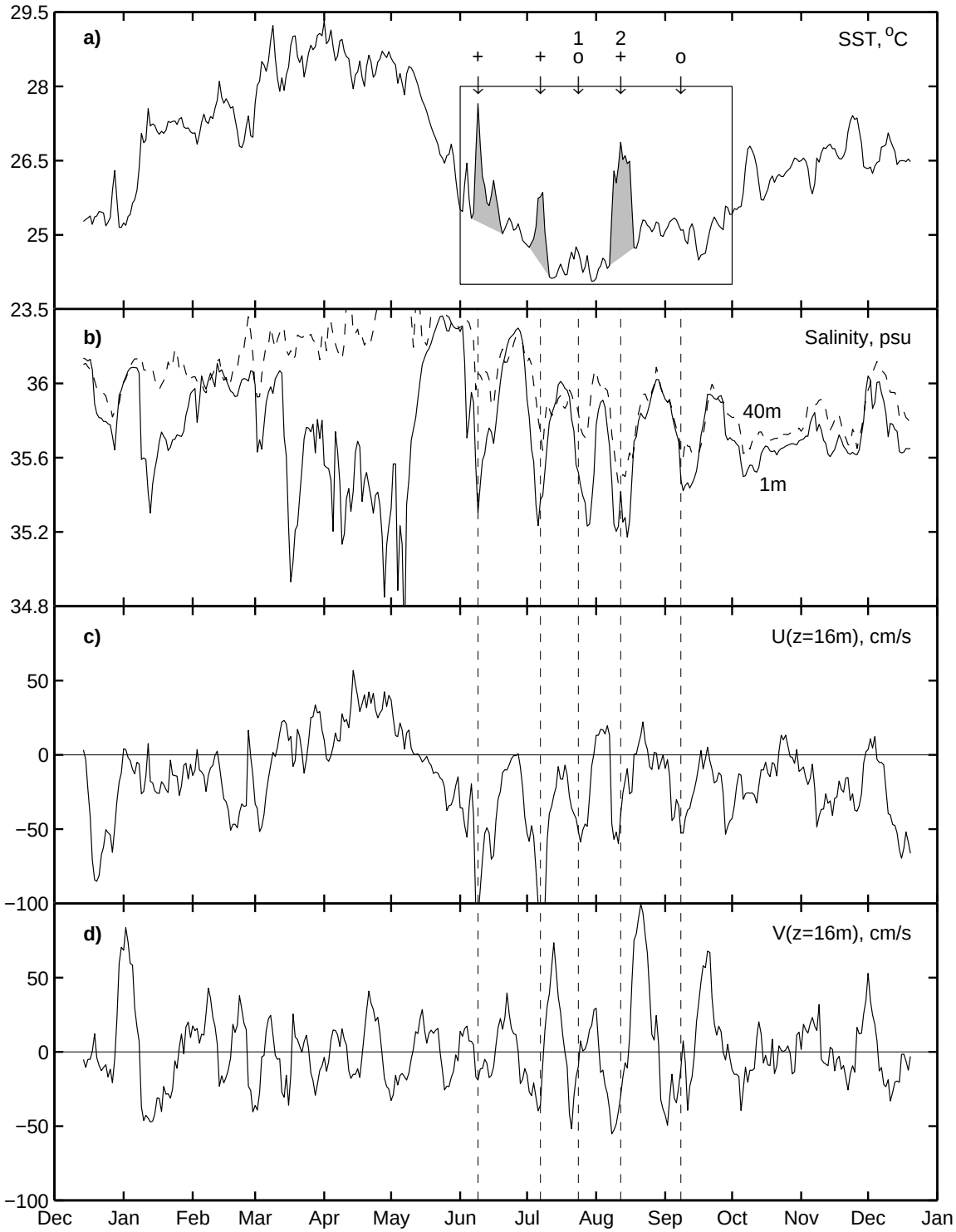

Figure 4. (a) SST, (b) sea surface and 40m-depth salinity, (c) zonal currents at 16 m depth, (d) meridional currents. Westward current surges during June-September are marked with arrows. Symbols (`+' and `o') mark events with stronger and weaker SST response, respectively. Numbers mark events illustrated in Fig. 8.

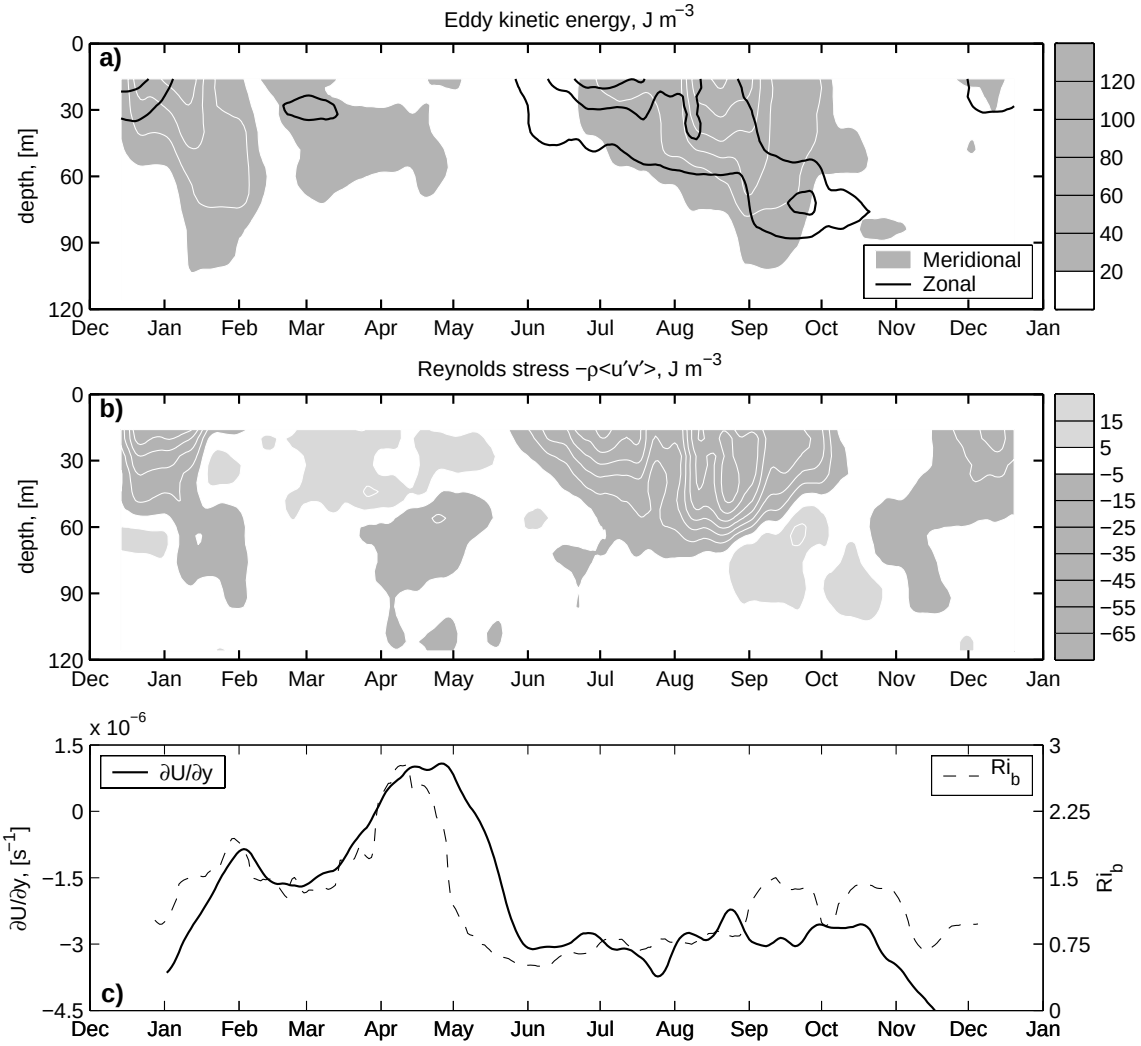

Figure 5. (a) Eddy kinetic energy of the zonal and meridional components. Isolines are drawn at 20 J m^{-3} intervals. Meridonal component values exceeding 20 J m^{-3} are shaded. (b) Reynolds stress. Isolines are drawn at 10 J m^{-3} intervals. Values greater than 5 J m^{-3} or less than -5 J m^{-3} are shaded in light and dark gray, respectively. (c) Meridional shear of the zonal current and bulk Richardson.

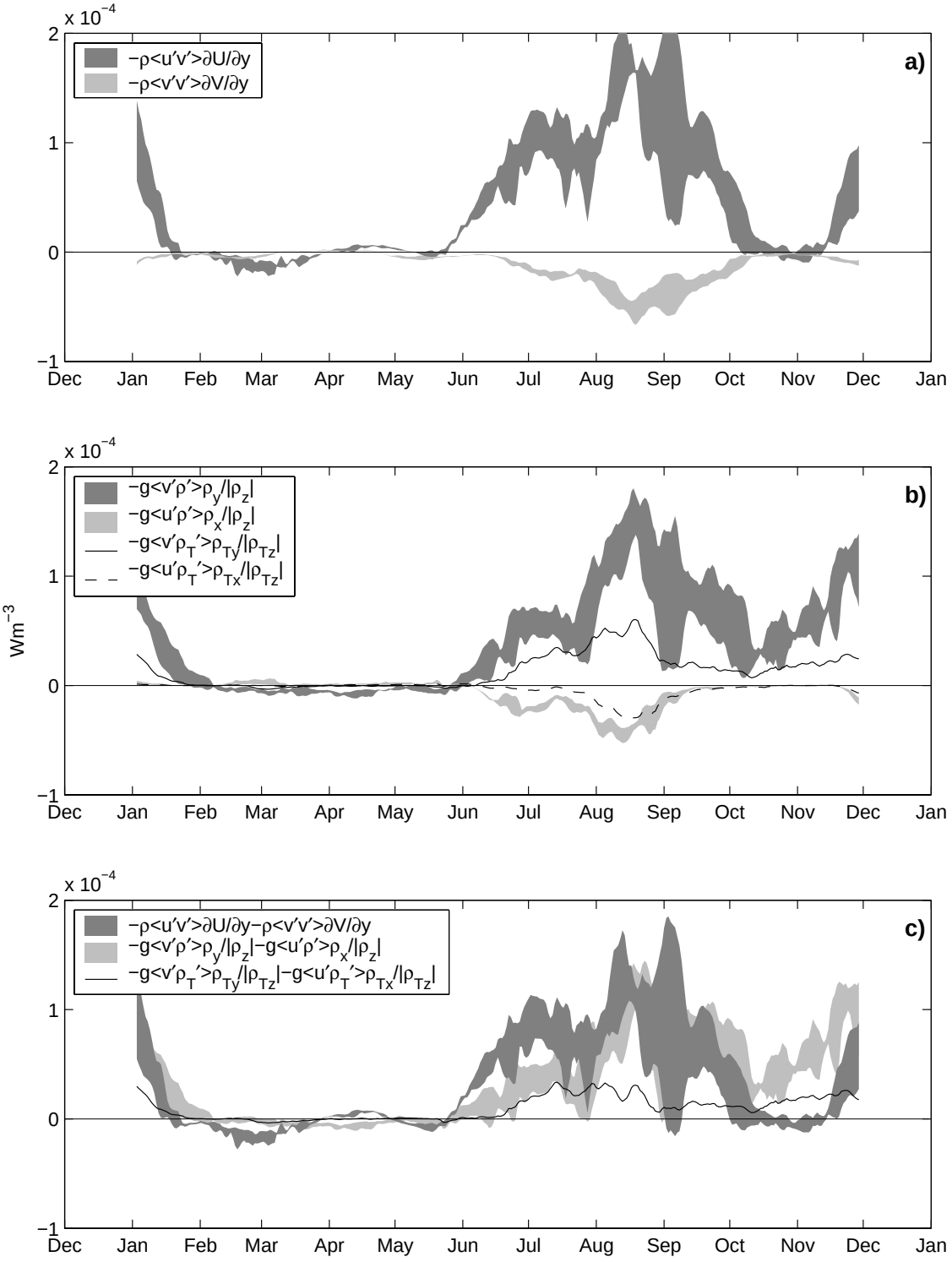

Figure 6. (a) Barotropic energy conversion averaged through the upper 40 m. Shadings bound the spread of estimates based on 20-day, 30-day, and 40-day running means. (b) The same as in (a) but for baroclinic conversion. Lines present estimates (marked with subscript "*T*" in the legend) based on temperature-only data computed with 30-day running mean. (c) Comparison of the combined barotropic and baroclinic conversions.

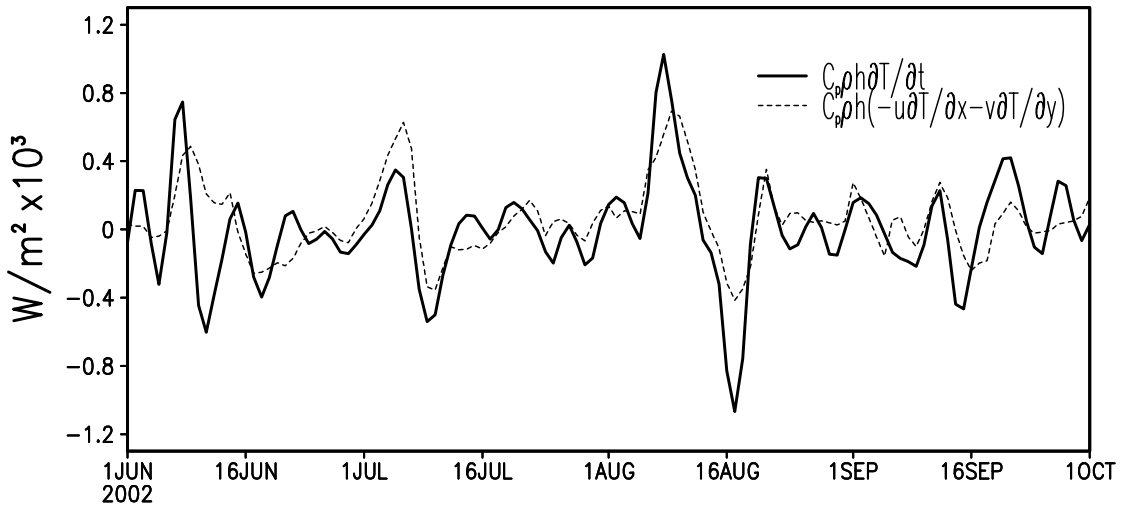

Figure 7. Three day averaged rate of change of the mixed layer heat content and horizontal heat transport.

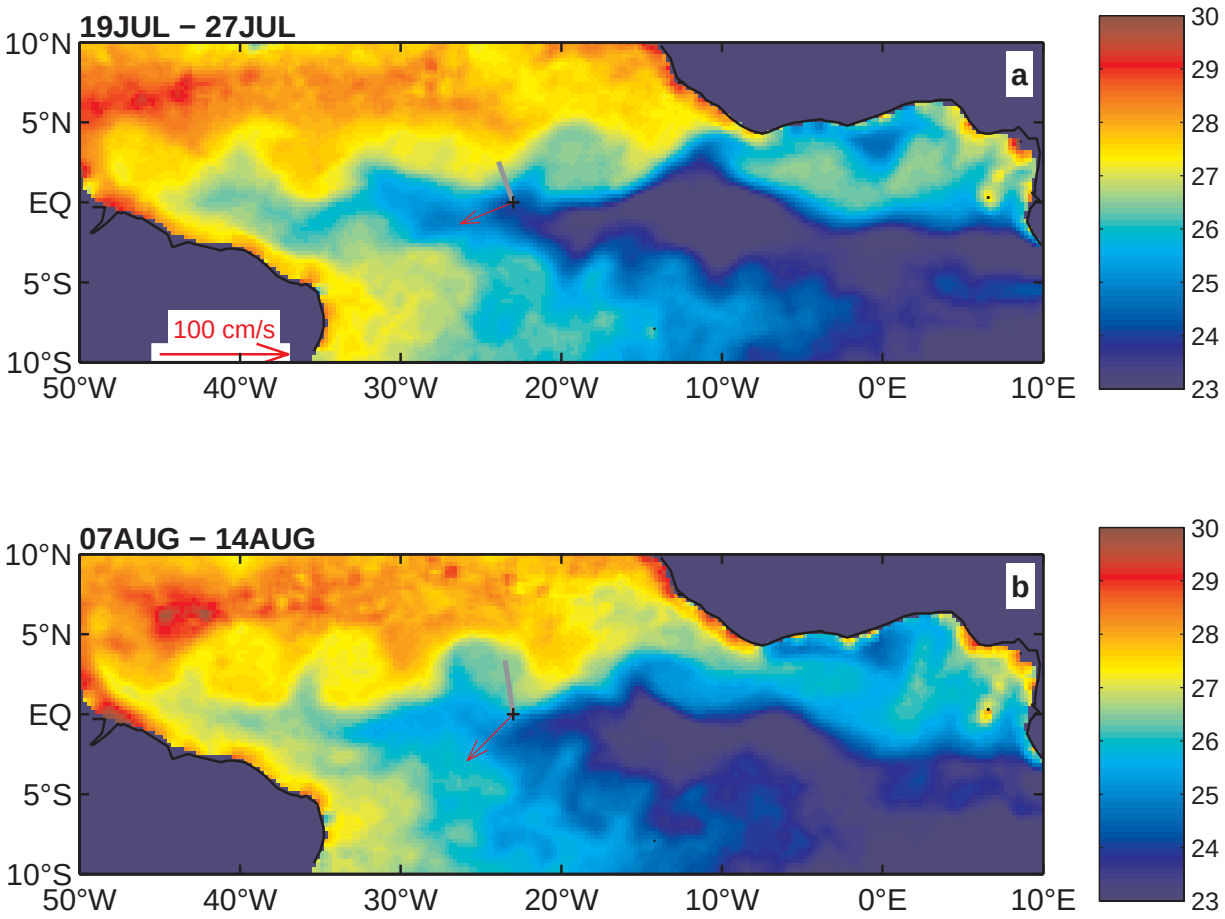

Figure 8. Tropical Atlantic SST (in ^{o}C) during (a) late July and (b) early August. Arrows and gray lines show currents at z=16m and direction of SST gradient, respectively.